Tellus (1994), 46A, 398–418
Printed in Belgium – all rights reserved

TELLUS
ISSN 0280–6495

An experimental coupled forecast system at the National Meteorological Center

Some early results

By MING JI*, ARUN KUMAR and ANTS LEETMAA, *Coupled Model Project, National Meteorological Center, NOAA/NWS, Washington, D.C. 20233, USA*

(Manuscript received 6 August 1993; in final form 25 April 1994)

ABSTRACT

An experimental coupled ocean-atmosphere model forecast system has been implemented at the National Meteorological Center (NMC) for routine multi-season climate forecasts. The ocean initial conditions for the forecasts are provided by an ocean data assimilation system which uses a basin model of the Pacific Ocean integrated with a four-dimensional variational data assimilation system. Pacific basin ocean reanalyses for the period 1982–1992 provided both the initial conditions and the verification fields for the coupled model forecasts. The coupled model consists of a modified T40 version of NMC's operational medium range forecast model coupled to a Pacific basin ocean general circulation model. Hindcast experiments starting on the first of every month from October 1983 to 1993 have been made to establish the skill of this system in forecasting sea surface temperature variability in the tropical Pacific with lead times of up to several seasons. The system consistently out performs persistence forecasts even at short forecast lead times, and is able to forecast most of the sea surface temperature variability that occurred in the tropical Pacific during 1984 to 1993.

1. Introduction

The largest natural climatic variability observed on the interannual time scale is the El Niño/Southern Oscillation (ENSO). This is the result of ocean-atmosphere interactions on the planetary scale. Remarkable strides have been made during the last decade in documenting its causes and impacts, and in developing coupled ocean-atmosphere models to simulate and study it. Representative of the modeling studies are those by McCreary and Anderson (1984), Cane and Zebiak (1985), Schopf and Suarez (1988), and Philander et al. (1989). The low frequency, large spatial scale, the strong coupling between the ocean and atmosphere in the Tropics, and the relevance of linear dynamics in the equatorial ocean, all suggest that ENSO predictions might be possible. Indeed a number of studies have demonstrated that prediction of the temperature anomalies in the eastern equatorial Pacific associated with the ENSO with statistical or dynamical models is feasible. Skillful forecasts are possible up to a year or so in advance (Cane et al., 1986; Barnett et al., 1988, 1993; Barnston and Ropelewski, 1992; Latif et al., 1993).

The development of a coupled ocean-atmosphere system for multi-season climate forecasting has been a research focus at NMC since early 1991 (Ji et al., 1994a). The objective has been to implement an operational multi-season forecast capability for that part of the climatic variability associated with ENSO. The memory of the climate system resides primarily in the ocean. The importance of this in the Pacific for ENSO has been shown by Wyrtki (1975; 1985) and Zebiak and Cane (1987). Hence the central need is to initialize the ocean component of the climate forecast

* Corresponding author.

system. The work at NMC has established the two main components of a coupled climate forecast system. The first one is an ocean analysis system which producing the oceanic initial conditions and verification fields for the forecasts. The second one is a coupled forecast model which consists of the ocean and atmosphere general circulation models (GCM) and an interface controller which governs the exchanges of heat, momentum and moisture fluxes at the air–sea interface.

Since the tropical oceans are predominantly wind forced, a common way of initializing the coupled forecast systems currently in use is to force the ocean component up to the time the forecast starts with the observed history of wind forcing (Cane et al., 1986). For coupled models that use a statistical atmosphere (Barnett et al., 1993), the anomalous wind forcing is derived from the past history of the sea surface temperature anomaly. However, there can be considerable error in these fields. Also the ocean models themselves are far from perfect. Much of the effort at NMC in the development of the ocean analysis system has focussed on producing ocean analyses that combine in situ data into an wind driven ocean general circulation model using data assimilation to minimize such errors. An earlier discussion of the ocean analysis effort was given in Leetmaa and Ji (1989). An up-to-date discussion of the current analysis system and the structure of the climatic variability that has taken place in the Pacific from mid-1982 to the present can be found in Ji et al. (1994b). Two Pacific basin ocean re-analyses for 1982 to 1992 have been produced using the ocean analysis system. These ocean analyses, in addition to documenting the climatic variability of the ocean, serve as ocean initial conditions for the coupled forecasts.

Our forecast system consists of a T40 version of NMC's operational medium range spectral forecast model (MRF) coupled to an active Pacific basin ocean general circulation model. The MRF model was developed for short to medium range weather forecast at NMC; hence adjustments to the model's physical parameterizations (tuning) were required in order to improve its tropical convection and to reduce model biases in the tropics during the longer integrations required for seasonal time scale forecasts. Many atmospheric GCMs have problems simulating robust tropical circulations; hence details of the tuning process are discussed in Section 2. In Section 3, we describe in detail of the coupled model, its coupling procedures and the oceanic and atmospheric initial conditions used for forecast experiments. Preliminary results from forecast experiments using our coupled model will be presented in Sections 4 and 5. Section 6 summarizes our conclusions.

2. The atmospheric model

The atmospheric part of the coupled forecast system is derived from NMC's operational Medium Range Forecast model (Kanamitsu et al., 1991). A T40 spectral resolution version of this is used in order to facilitate longer integrations that are required for climate studies. Relative merits of T40 against higher horizontal resolution in the simulation of atmospheric circulations and the surface fluxes have been discussed by many authors (Tibaldi et al., 1990; Boyle, 1993). This resolution captures much of the physical and dynamical behavior of models with higher resolution. The model climate for the NMC model at T40 resolution also has been investigated by several studies (Kanamitsu et al., 1990; Van den Dool and Saha, 1993; Ebisuzaki and Van den Dool, 1993a). An example of the mean of the September, October and November (SON) surface wind stress and precipitation in the Pacific for the T40 model are shown in Fig. 1. The mean surface stress and precipitation are obtained from the Atmospheric Model Intercomparison Project (AMIP) experiment using the NMC's T40 model (Ebisuzaki and Van den Dool, 1993b) in which the physical parameter settings are similar to the NMC's operational MRF model. In the equatorial Pacific and east of the date line, stresses from the AMIP T40 model (1a) are much weaker than climatological estimates (Hellerman and Rosenstein, 1983; Harrison, 1989). The model values at near 140° W average around 0.04 N/m^2, whereas the climatological estimates are near 0.08 N/m^2 (not shown). Considerable experience with the ocean model in data assimilation studies indicates that in order to maintain the east–west pressure gradient in the equatorial ocean, a surface stress which has magnitude at about 90% of the climatological stress produced by Hellerman and Rosenstein (1983) is necessary. If the ocean were forced with stresses of the magnitude shown in

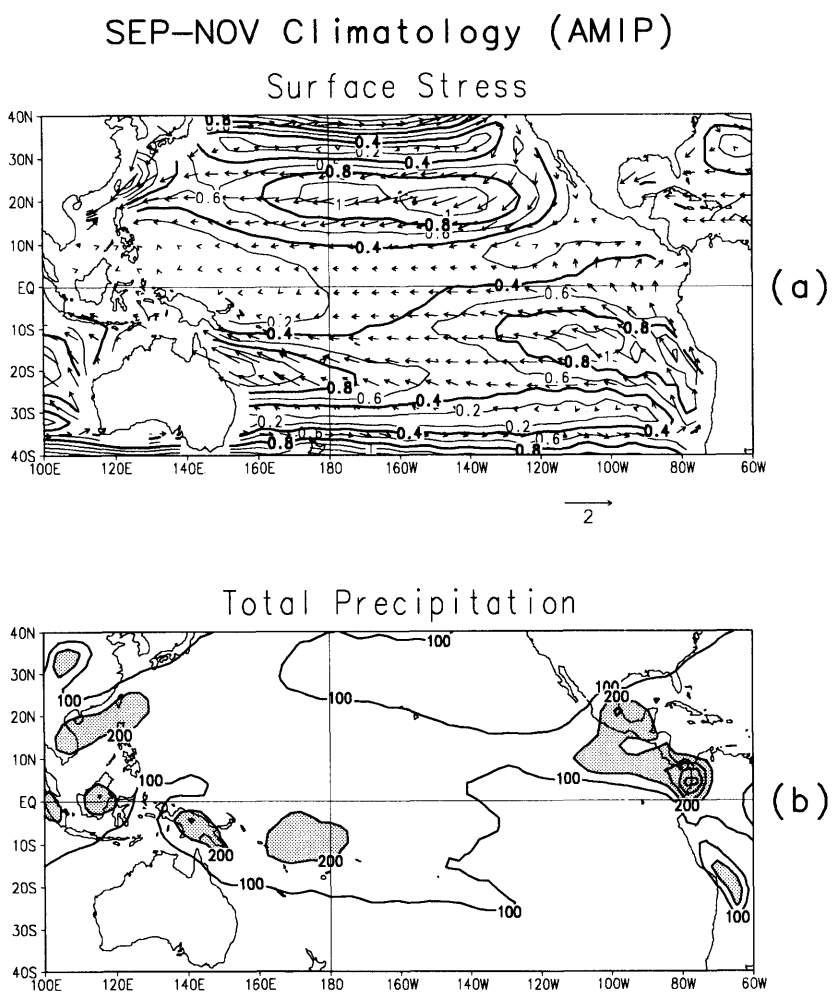

Fig. 1. T40 MRF model climatology for September to November (SON) average from the AMIP experiment. (a) Surface stress in N/m^2, contour interval is 0.04; (b) total precipitation in 0.001 m/month, contour interval is 100, regions greater than 0.2 m/month are shaded.

Fig. 1a, the oceanic pressure gradient and the magnitude of the equatorial upwelling in the eastern Pacific, which maintains the cold tongue, would be significantly weaker than what is normally observed. Hence the simulated mean ocean state would resemble an El Niño.

The weaker than observed easterly stresses in the AMIP version of the MRF, and in many other atmospheric models (Reynolds et al., 1989), are to a great extent linked to the spatially diffuse nature of the model generated precipitation field (1b). The heating field resulting from such a precipitation distribution, due to its weak horizontal gradients, does not provide enough equatorward acceleration to the Trade wind flow. The implications of subtle changes in the tropical surface pressure field on the surface wind distribution have been discussed by Lindzen and Nigam (1987). Alternatively, a weak tropical precipitation field results in a weak top of the boundary layer upward vertical velocity field, the consequences of which on the surface stresses are reported in Neelin (1988). It can be argued that a more tightly organized tropical precipitation field, via small changes in the

surface pressure distribution, can lead to enhanced low latitude surface winds and more appropriate forcing fields for ocean models in this region.

Convection, boundary layer processes, and radiative processes are interrelated in a complicated manner in producing the near-equatorial circulations and rainfall patterns. Extensive numerical experiments were carried out to develop a modified T40 version of the MRF for climate forecasting which would produce more realistic simulations in the tropics. The primary focus of these was to improve the surface stresses. This involved close examination of the impact on the T40 MRF model climate to changes in various physical parameterizations. However, the form of the physical parameterizations was maintained in order to have a model which closely resembled the operational MRF.

2.1. The convective parameterization scheme

The deep convection parameterization in the MRF is based on the Kuo type scheme (Kanamitsu, 1989). (In July 1993 this was replaced in the operational MRF model by a version of the Arakawa Schubert scheme.) A particular feature of its implementation in the MRF is the screening of all the model grid points for the possibility of convection. This procedure is performed based upon some predefined set of conditions (NMC Staff, 1988). Of most importance is the necessary (but not sufficient) requirement that for deep convection to be present at a grid point, the large-scale moisture convergence should exceed a prescribed threshold. The moisture convergence is the sum resulting from surface evaporation and the dynamical convergence. Average evaporation in the Tropics is close to 0.003 m/day (about 100 W/m^2). Hence unless there is strong large-scale moisture divergence, for low values of the moisture convergence threshold, for example 0.002 m/day, the tropical atmosphere will always be close to producing convection. Further, this condition while governing the location of the convection, also controls the ratio of the convective versus the large-scale precipitation. In general a larger value of the required moisture convergence threshold will make the deep convection less likely to occur. For a nearly fixed amount of global rainfall, which generally is the case, this leads to enhancement of the large scale precipitation. The reverse occurs if the moisture convergence requirement is reduced.

For small values of the required moisture convergence threshold, considering also the effects of local evaporation, the air parcels in the Trades are likely to go through the process of convection before reaching low latitudes. This is the likely cause of the spatially diffuse model precipitation climatology shown in Fig. 1b. A larger value for the required moisture convergence threshold will force the parcels to reach lower latitudes before convection can take place. Reduced convective precipitation, locally, does not necessarily have to be compensated by increased large-scale precipitation since convection does not require the ambient atmosphere to be saturated while large scale precipitation does. Thus a higher value of the moisture convergence threshold might lead to better more tightly organized tropical convection patterns. Concentrated heat source would lead to a more vigorous low level circulation, e.g., stronger surface stresses.

A similar procedure involving the cloud work function for the Arakawa-Schubert scheme has been reported by Sud et al. (1991). The value of the moisture convergence threshold cannot be raised indefinitely since this will lead to complete shut off of the deep convection and alter the vertical heating structure of the tropical low latitudes. The importance of the vertical heating structure in the simulation of tropical mean climate, intra-seasonal variability, and tropical mid-latitude teleconnections has been noted by many investigators (Meehl and Albrecht, 1991; Lau and Peng, 1987; Hartman et al., 1984).

Initial experiments with higher values of the moisture convergence threshold did result in improved spatial definition in the tropical convection and stronger surface stresses. But they also showed a tendency of producing grid point storms. This should be expected since a higher value for moisture convergence criterion will tend to prefer the grid points with already well developed vertical motion associated with existing convection. Since the Kuo scheme, due to the exclusion of the down drafts, lacks a direct mechanism to modify the properties of the underlying boundary layer, the self-limiting behavior of convection (at certain geographic locations, such as islands, not associated with moving tropical disturbances) is not very active. To confine the oceanic convective rain-

fall to lower latitudes and at the same time not create grid point storms, within the limitations of the numerical model, a better screening criteria for convection was needed. For this reason, the moisture convergence criterion from the convective parameterization scheme was removed. Instead, a condition based upon the difference between the surface equivalent potential temperature (θ_e) and the θ_e at 300 hPa was added. This condition is a measure of bulk tropospheric conditional instability. The relationship between the positive low values of the gross moist static stability and the positioning of the deep convection in the tropics has been discussed by Neelin and Held (1987). Further, in the tropical latitudes, low-level inversions play a critical rôle in regulating the convective activity (Kloesel and Albrecht, 1989). Due to coarse vertical resolutions in the atmospheric boundary layers and errors in the parameterization schemes, these low level inversions are not well simulated. Lack of reasonable simulation of the inversion results in the absence of an important selection mechanism to guide the spatial location of the deep convection. In view of the aforementioned model deficiency, the new condition, i.e., the θ_e test, acts as the proxy and tries to compensate for the lack of reasonable simulation of the tropical low level inversions. This condition

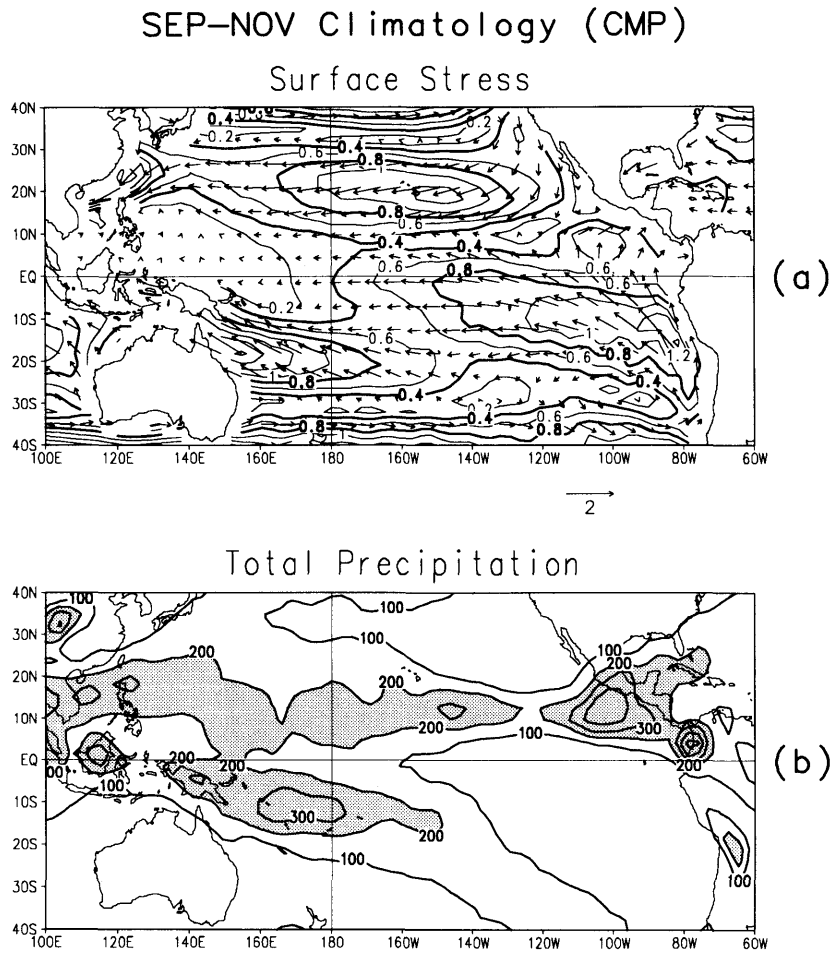

Fig. 2. Same as in Fig. 1, but from the modified T40 MRF (CMP) model.

has the added advantage that it does not depend on the model's horizontal resolution.

For the version of the atmospheric model used in these coupled experiments, the moisture convergence criteria was relaxed and replaced with the check that the surface θ_e exceeds the θ_e at 300 hPa by 5 K. This particular numerical value was chosen from the T40 MRF model climatology and taking into account that the convection should be more likely to occur over the warmer oceans of the tropical low latitudes. The surface wind stress and the precipitation for SON with the modified T40 MRF (CMP) are shown in Fig. 2. East of the date line, near equatorial surface wind stresses (2a) show marked strengthening and are closer to the observed climatological estimates. This to a large extent is a direct response of the changes in the model's precipitation climatology (2b) which for the modified version show a better near equatorial organization. (This simulation also includes the other parameter changes that are discussed in the following sections.)

2.2. *Vertical diffusion in the free atmosphere*

In the MRF the asymptotic mixing length for temperature (T), specific humidity (q), and momentum is set to 250 m (NMC Staff, 1988). One of the obvious shortcomings of the model simulations was the enhanced air–sea temperature differences in the tropics. These averaged around 1.5°C whereas climatological atlases suggest values of 0.5 to 1.0°C. Most aspects of air–sea exchanges are sensitive functions of this temperature difference because of the stability dependence of the exchange coefficients. Attempts were made to increase the near surface air temperatures. In principle this could be achieved by reducing the vertical diffusion of temperature. This would result in the air temperatures staying closer to the underlying sea surface temperatures (SST). However, simultaneous reduction of the asymptotic mixing lengths for moisture and temperature lead to a further reduction of the air temperature. This resulted from vertical changes in structure of the low-level moisture leading to an increase in the low-level long-wave cooling, which offsets any change resulting from a reduced diffusion of temperature. After extensive experimentation, values of 10 m and 30 m were chosen for the asymptotic mixing lengths of T and q, respectively. Observational evidence for such small values for the mixing lengths, at least in a stable atmosphere, have been reported by Kim and Mahrt (1992). Fundamental differences between the vertical diffusion of moisture and other scalar variables have been noted by Holtslag and Moeng (1991) and Troen and Mahrt (1986). This might encourage the use of different eddy diffusivities for T and q.

The asymptotic mixing length for momentum was increased to 500 m. This modification was incorporated to enhance the strength of the surface winds. A larger value of the vertical mixing with a constant horizontal pressure gradient force in the vertical, will provide smaller deceleration at the bottom of the boundary layer and would result in an increase of the surface winds.

The changes required in the mixing lengths indicates the complex interactions between the different parameterization schemes used in the GCM. Changes in one parameterization can have unexpected impacts and might require compensatory changes in the other schemes. This statement is of most validity in the context of models which under the constraint of several imperfect parameterization schemes are called upon to simulate widely varying atmospheric conditions.

2.3. *Cloudiness parameterization*

Interactive clouds were only recently introduced into the MRF, and the cloud simulations can be improved upon. In the standard T40 MRF model, the total cloudiness was greatly underestimated. This resulted in too much shortwave energy reaching the ocean surface. To overcome this problem, the low-level stratiform cloud amount parameterization was changed to follow Slingo and Slingo (1991). Compared to the MRF, in regions of upward motion, the modified procedure has a weaker vertical velocity filter and allows larger amounts of cloudiness to be present. The maximum impact of this modification is in the mid-latitude frontal regions. In the subsidence regions the dependence of the low level clouds on the inversion strength was taken to be

$$-25\mathrm{d}\theta/\mathrm{d}p - 2.25,$$

where θ represents potential temperature and p represents pressure.

The constants appearing in the above expression are different from the ones used in Slingo and

Tellus A/46/4-5

Slingo (1991) and are chosen based on the inversion strength climatology produced by the modified T40 MRF. No stratiform clouds in the subsidence region exist if at the top of the boundary layer

$$d\theta/dp > -0.09 \text{ K hPa}^{-1}.$$

In the MRF, since the low level convective clouds override the cloudiness information provided by the low level stratus clouds, in the tropical region, unrealistically low cloudiness amounts tend to be associated with moderate precipitation rates. To enhance these cloud amounts, the amount of low level clouds, CL, resulting from the convection was altered to

$$CL = 1.25(a + b \ln P)$$

where a and b are empirical constants and P is the precipitation rate. The constant 1.25 is different than the one used in the operational MRF. The modified cloudiness parameterizations, compared to the original scheme, produces a larger amount of clouds and considerably reduces the excessive surface downward short-wave flux.

It should be pointed out that most of the surface flux errors do not have much impact upon the medium range forecast since they are run with non-interactive oceans. For example, excessive surface shortwave flux at the ocean surface, without any energy balance requirement does not lead to sea surface temperature (SST) bias. Further, since to first approximation, clouds act as reflecting bodies, any errors in their amounts does not have substantial impact on the atmospheric heating rates (to which medium range forecast would be most sensitive). On the other hand these changes, if introduced into the MRF, may not be beneficial for the medium range forecast. A clear example is the change in the convective parameterization scheme, which if introduced into the model, while adjusting to a different rainfall climatology, demonstrates a large spin up in rainfall. A feature not desirable for the medium range forecast.

3. The coupled model

The atmospheric component of the coupled model has been described in the Section 2. The ocean component of the coupled forecast model consists of an ocean GCM originally developed by Bryan (1969) and Cox (1984) at GFDL, and subsequently modified by Philander et al. (1987). Its domain consists of the Pacific basin extending from 45°S to 55°N and from 120°E to 70°W. The zonal resolution is 1.5°, and the meridional resolution is 1/3° within 10° of the equator. Outside the equatorial zone the meridional resolution decreases gradually to 1° by 20°N and 20°S. The model has 28 vertical levels. The vertical mixing is provided by a Richardson number formulation (Pacanowski and Philander, 1981).

3.1. Coupling procedures

Despite the effort that went into modification of the atmospheric model, deficiencies in the flux fields remained, which had an impact on the ocean SST forecasts during coupled model integrations. Assuming an average depth of ocean mixed layer of 40 to 50 m, a 15 W/m^2 net heat flux error could result in a SST error of 0.2°C in a 1-month integration in the absence of negative feedbacks between ocean and atmosphere. This could result in a SST error of 2°C during a 10-month integration. In reality, in some areas, net heat flux errors could significantly exceed 15 W/m^2 and feedback among SST, heat flux and convection could make matters much worse. Thus at present, the exchanges of fluxes at the air–sea interface are done in a combination of full and anomaly coupling. Anomaly coupling is needed for the net shortwave flux and the stress at the ocean surface. For the shortwave radiation this was necessary because, despite improvements, the interactive cloud scheme in the atmospheric model was still unable to accurately simulate the mean annual variation at the ocean surface. As for the stress in the near equatorial zone, the atmospheric model's easterlies were too weak during the late winter and spring. Hence, if full coupling were used, this would lead to El Niño like conditions every year at that time.

The short-wave flux and stress anomalies were computed by subtracting the atmospheric model's climatology from the instantaneous fields for these quantities. The atmospheric model's mean annual cycles were generated when the atmospheric model was integrated for 11 years, forced with observed SSTs, for the period of 1982 to 1992. The full stress and shortwave flux fields that were used to force the ocean during the coupled simulations were

obtained by adding these anomalies to prescribed climatologies. The prescribed stress climatology is that of Hellerman and Rosenstein (1983) reduced by 10%. The prescribed short-wave climatology was computed using the bulk formula from Reed (1977) and estimates of the mean annual cycle of cloudiness from the International Satellite Cloud Climatology Project (ISCCP).

In essence, full coupling was used for sensible, latent and long wave fluxes. However, adjustments were made to reduce the systematic bias in the SST forecasts (described in a later section). We believe that the air–sea temperature differences that this atmospheric model produces are about 0.5°C too large. Hence corrections were made to the latent and sensible fluxes. The former was reduced by 10%, and an addition of 10 W/m^2 was made to the sensible heat flux. An additional flux correction, based on the convective rainfall rate within 10° of the equator, was imposed to account for cooling of the ocean surface by the rain. This produces an additional cooling on the order of 10 W/m^2. Even with the anomaly coupling, the simulation of the variations in the short wave flux are not well done. This correction partly corrects for this problem. Clearly there is a lot of physics that takes place in the convective areas which is not simulated well by these models.

The exchanges of fluxes and SST information between the ocean and atmosphere take place every 5 days in these experiments. Initially the coupling was performed daily. However, early results suggested that the higher frequency stress forcing generated energetic high frequency motions in the ocean which produce numerical problems. It was not clear that the Richardson number based vertical mixing scheme was the most appropriate one to use with this frequency of forcing. Hence the longer coupling interval was chosen. In retrospect it is not clear whether these conclusions are correct. The sensitivity of the forecasts to the coupling frequency and the vertical mixing schemes are areas we need to examine in the future.

3.2. Initial conditions

The first of the ocean reanalyses which produced the initial conditions for our forecasts, used the Hellerman and Rosenstein (1983) climatology combined with the stress anomalies produced by the atmospheric model forced with observed SSTs for the same period. The second one used the Harrison (1989) climatology, and additional quality control was applied to the observed data. Subsurface thermal data from the current meter moorings in the equatorial Pacific from 1982 through 1992, which were not available for the first reanalysis, were also included. The procedure of anomaly coupling reduces the potential for climate crash to occur at the start of the forecast. This results when there is a mismatch between the stress produced from the atmospheric model in the coupled system and the oceanic pressure gradients in the ocean initial conditions. Since many atmospheric models produce easterlies that are too weak in the near equatorial zone, this would lead to a partial collapse of the oceanic east–west pressure gradient during the first few months of the coupled model integration and an El Niño would result in almost every forecast. This clearly presents a problem for forecasts of a few seasons in length.

The initial conditions for our experimental forecasts were taken from these reanalyses. The time evolution of the anomaly in the depth of the 20°C isotherm along the equator from the second reanalysis is shown in Fig. 3. The regular progression of interannual variability is clearly evident. The three major warm episodes, i.e., during 1982–83, 1986–87, and 1991–92, feature positive depth anomalies, while the two cold episodes, 1984–85 and 1988–89, are characterized by negative anomalies. The anomaly signals appear to irregularly propagate eastward with an average phase speed of about 0.5 m/s, which is much less than that associated with individual Kelvin wave packets (about 3 m/s). This reflects the impact of coupled interactions between the ocean and atmosphere. Instantaneous oceanic conditions from the reanalyses were saved at monthly intervals to serve as initial conditions for the forecast experiments. However, time averaged oceanic fields which may contains fewer high frequency oceanic transients, might serve better as ocean initial conditions for the coupled model. This will be investigated in the future.

Multiple simulations using atmospheric model alone forced with observed SSTs for 1982 to 1993 were made, and monthly atmospheric model restart files were saved from these simulations. These monthly atmospheric model restart files are used as the atmospheric initial conditions for the coupled model forecasts.

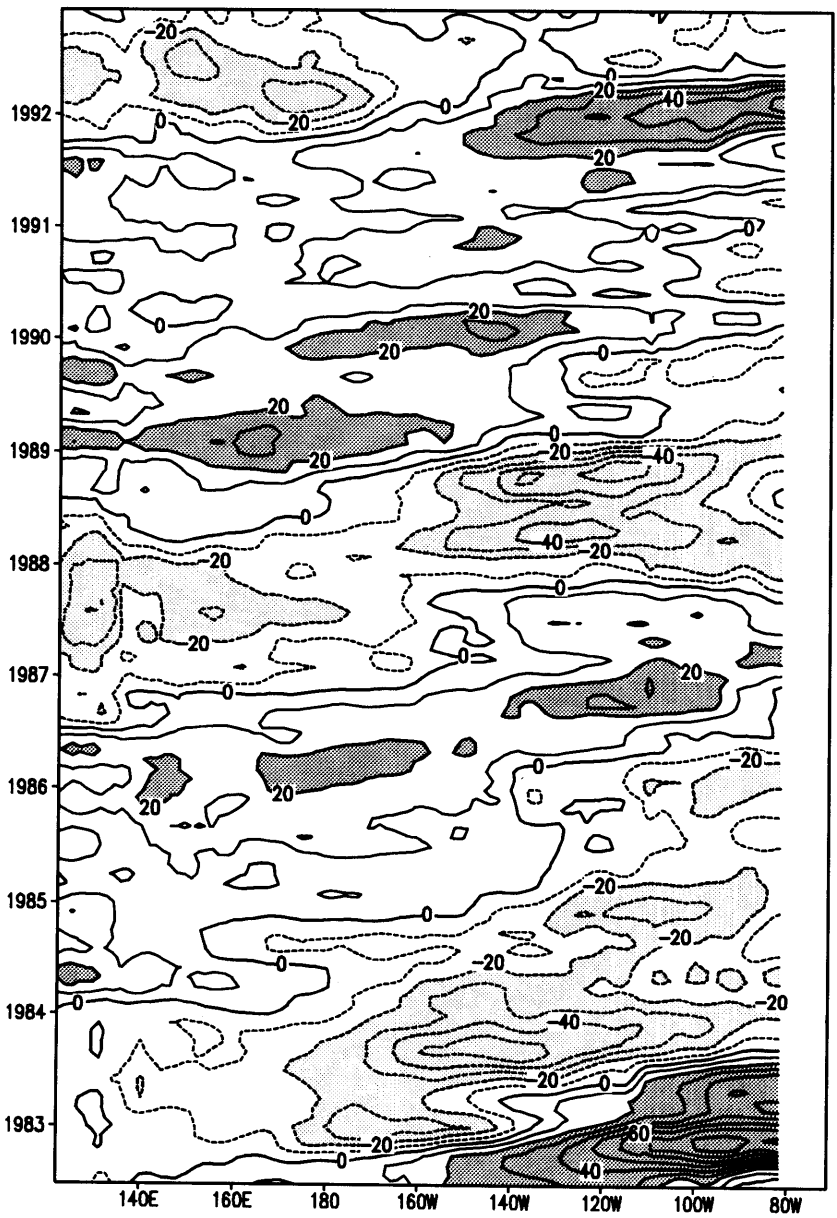

Fig. 3. Anomalous depth of the 20°C isotherm along the equator in the Pacific. The mean annual cycle for this period has been removed. Contour interval is 10 m.

4. The coupled forecast experiments

The initial objectives of the coupled forecast experiments were limited. The intent was to see how well the system could forecast northern winter SST anomalies in the tropical Pacific with various lead times. With this purpose in mind, forecast experiments were performed initially starting on the first day of March, May, June, July, August, October, and December from October 1983 through 1992. Subsequently, additional forecasts starting from all other months for the same period were completed. Each experiment was carried out for up to 12-month forecasts of monthly SST anomalies.

To verify these forecasts, monthly blended analyses for sea surface temperature produced at NMC for TOGA (Reynolds, 1988; Reynolds and Marsico, 1993) was used. A skill score was computed using point correlations between the observed time series of SST anomalies and the predicted anomalies at all geographic locations in the tropical Pacific domain. Observed SST climatology is used to compute for both observed and forecast SST anomalies. This was computed for monthly and seasonal anomalies. The primary season of interest was winter, e.g., December, January and February (DJF). The resulting anomaly correlation coefficients (ACC) at each grid point indicate the skill score of the forecast at each location. A score of 1.0 indicates that the anomalies were perfectly predicted. Before the skill scores were computed, a monthly systematic model bias was subtracted from the predicted SST fields. The monthly systematic bias is defined as average monthly SST difference between forecasts and observations for all forecasts starting from the same month of all years, and having the same forecast lead time. Thus, it is the difference between the coupled model climatology and the observed climatology. Further more, the systematic bias is a variable of forecast starting month. This takes into account of growth of the errors with forecast length. However, combination of bias fields of different starting month is possible, this will be illustrated below.

An example of the spatial distribution of the mean bias for November computed from all the runs starting in the previous summer (May through August) is shown in Fig. 4. The equatorial region from 10° N to 10° S tends to be warm except for a small region south of the equator in the far eastern Pacific which is a region dominated by upwelling. Flanking the equatorial region in the eastern Pacific are regions where the positive error exceeds 1.0°C. Poleward of 10° the average error is negative with an amplitude of as high as 1.0°C. A narrow band north of the equator in the eastern Pacific has positive error exceeding 1.5°C. This is also consistent with the maximum mean bias error in the Niño-3 region found during late fall to early winter (see below). This large model error may be

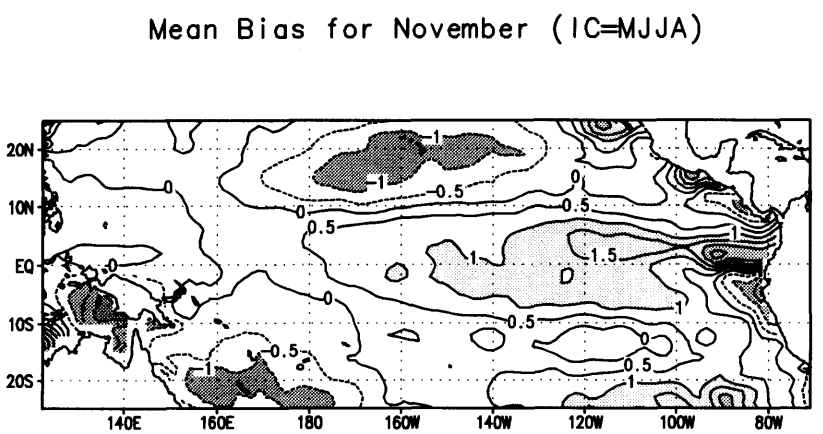

Fig. 4. Average systematic SST error for November for forecasts initiated on 1st May, June, July, and August. Contour interval is 0.5°C, warm bias above 1.0°C and cold bias below 1°C are shaded.

an indication that the strength of the equatorial upwelling in the fall is weaker in the model. Another possible reason may be partially due to the lack of resolution of the Blended SST analysis. In the fall season, the equatorial upwelling is at its maximum strength and results in a zone of strong horizontal temperature gradient just north of the equator. The Blended SST analysis has resolution of two degrees with substantial smoothing and is unable to resolve sharp frontal zones (Reynolds, 1988; Reynolds and Marsico, 1992). This may result in large difference between the model and the SST analysis. The mid-summer and the mid-winter bias also show a similar pattern, however, the narrow band of maximum positive bias region north of the equator in the eastern Pacific is much less noticeable in late winter patterns. This is probably because the equatorial upwelling has significantly subsided in the winter to spring period, reducing the thermal gradient north of the equatorial cold tongue.

Shown in Fig. 5 is the temporal evolution of the model biases for the Niño-3 region (150° W–90° W and 5° S–5° N). Model bias computed for all forecasts having the same starting month is depicted as an individual curve, the beginning point of the curve in the figure indicates the starting month of these forecasts. Model bias for all starting month from January to December are shown in the figure. Initial biases are generally less than 0.5°C. They all become more positive with time. For the forecasts from spring and summer into winter, the amplitude consistently peaks in late fall and then starts to decrease. For forecasts from late fall and winter into summer, the model exhibits cold systematic biases initially, the errors then turn to warm biases and increase rapidly to plateau around 0.5°C by summer.

Peak warm bias of over 1°C observed in the fall season, almost regardless of the forecast starting month, suggests that our model is probably unable to simulate the observed strength of the equatorial

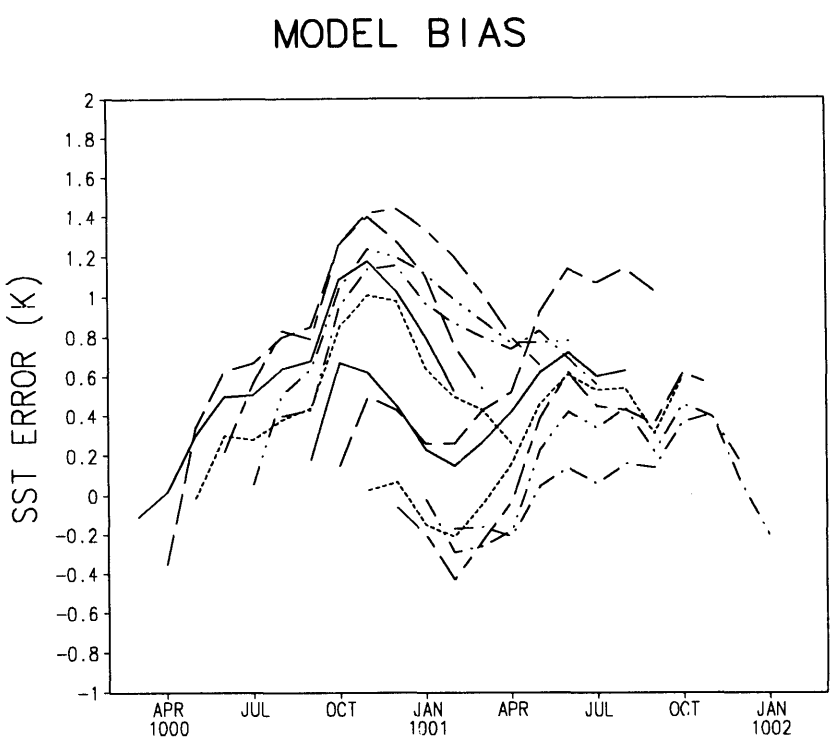

Fig. 5. The average systematic SST error in the Niño-3 region (150° W–90° W, 5° N–5° S) for forecasts of different starting month. Each curve represents the growth of the systematic errors for all forecasts starting from a given month.

upwelling in the fall season. This probably is an indication that for the fall season, the surface stress is still too weak in our model. It is also possible that the Richardson number based vertical mixing scheme used in the ocean model (Pacanowski and Philander, 1981) is not efficient to mix the surface momentum flux down to below.

An example of the comparison between the observed and forecast anomaly is shown in Fig. 6 for the warm event which took place during winter (DJF) 1991–1992. This was an average of three monthly forecasts for December, January and February 1991–1992 initialized on the 1st day of June, July, and August of 1991, respectively. Therefore, this is a 6-month lead forecast. Although the amplitude of the predicted anomaly appears excessive, the spatial structure of the warming that occurred during this time was reasonably well predicted. The anomaly correlation coefficient between observed and predicted anomalies is 0.83. Similarly, a 6-month lead forecast for the cold event of winter 1988–1989 is shown in Fig. 7. In this case the amplitude was better predicted. The anomaly correlation coefficient in this case is 0.73.

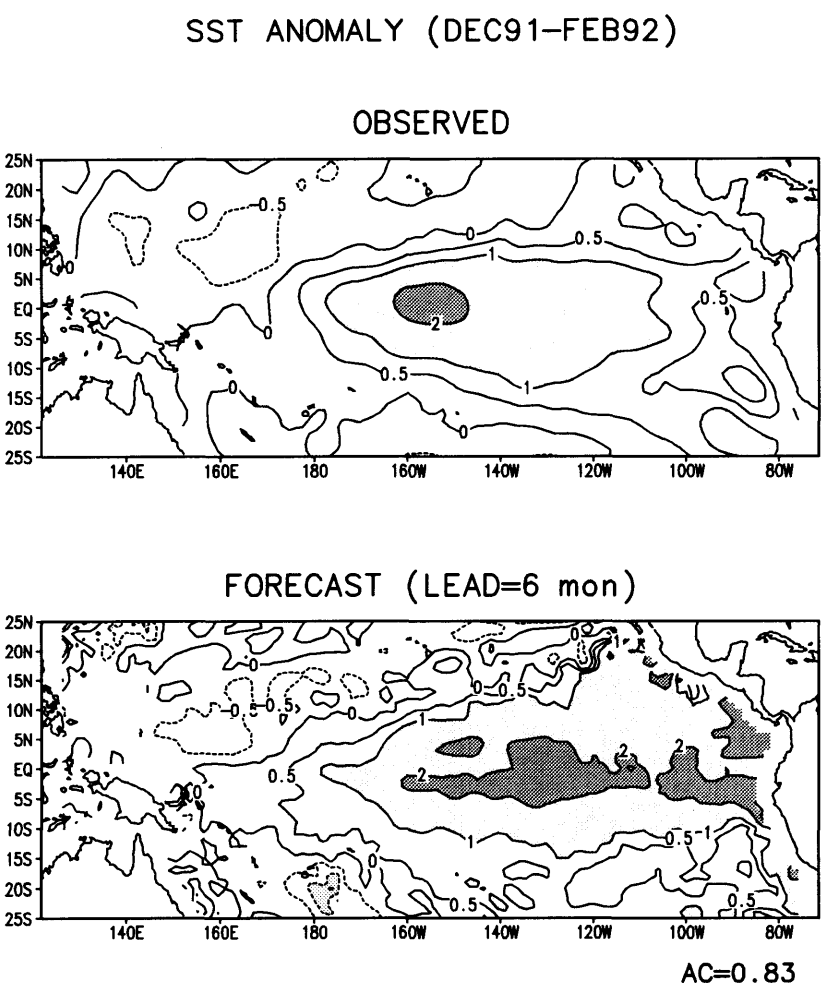

Fig. 6. Observed sea surface temperature anomaly field for the December–February 1991/92 period (6a), and predicted SST anomaly from the coupled model for the same period (6b). The predicted SST anomaly is a 6-month lead forecast (See text). Contour interval is 0.5°C.

Observed anomaly for the forecast period was not used in computing the model bias correction in both of above examples as if they were in an actual forecast situation. Examination of all the forecasts for DJF for the years 1984 to 1993 show that the coupled forecasts reasonably simulate the SST variability that occurred during this time with lead time of about 2 to 3 seasons.

Overall point correlation skill scores for the winter season (DJF) forecasts from our coupled model with lead time of six month are shown in Fig. 8. Fig. 8a shows the score for the coupled model forecasts and Fig. 8b shows the score for persistence forecasts. The latter is computed by persisting the observed monthly mean SST anomalies that occurred 6 months earlier into the following December, January or February for the years 1984 to 1993 and then computing the point correlations as indicted before. The dark shaded area shows regions where the correlations are above 0.9, i.e., over 81% of the variance is accounted for. This figure also shows that over the region where there is skill, the forecasts from the coupled model have significantly out performed the persistence at this lead time. The regions with highest skill are located in the central Pacific and

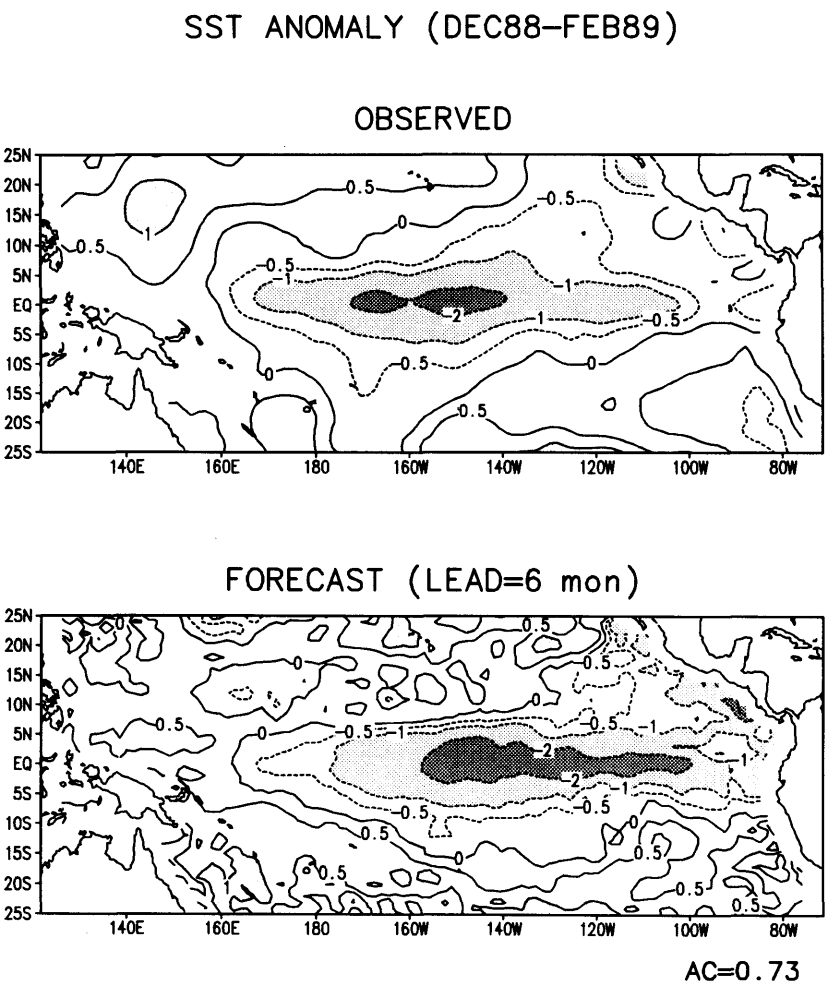

Fig. 7. Same as in Fig. 6, but for the December–February 1988/89 period.

are within 10° of the equator. In the southeastern Pacific persistence skill is comparable to those from the forecasts.

Shown in Fig. 9 are the forecast skill scores for lead times of 6 months (9a), 3 months (9b) and zero months (9c), regardless of the month the forecast was made for. The persistence skill scores for the corresponding lead times are shown in Fig. 10a–10c, respectively. A zero lead forecast for the model is the first month forecast; whereas for the persistence, it is the one month lag auto correlation coefficient. The skill levels for the 6-month lead time forecasts are reduced for both persistence and the forecasts in general, suggesting that other seasons may be more difficult to forecast for. Most of the skill for the model remains in the region within 10° of the equator and is more concentrated in the region just to the east of the date line. The low skill in equatorial eastern Pacific for persistence shows the difficulty in forecasting the near-equatorial region of strongest upwelling. In general, as the lead time decreases, the forecast skills for both the coupled model and the persistence increase. At 3 months lead time, the coupled model forecasts (9b) still out performs the persistence forecasts (10b) rather significantly,

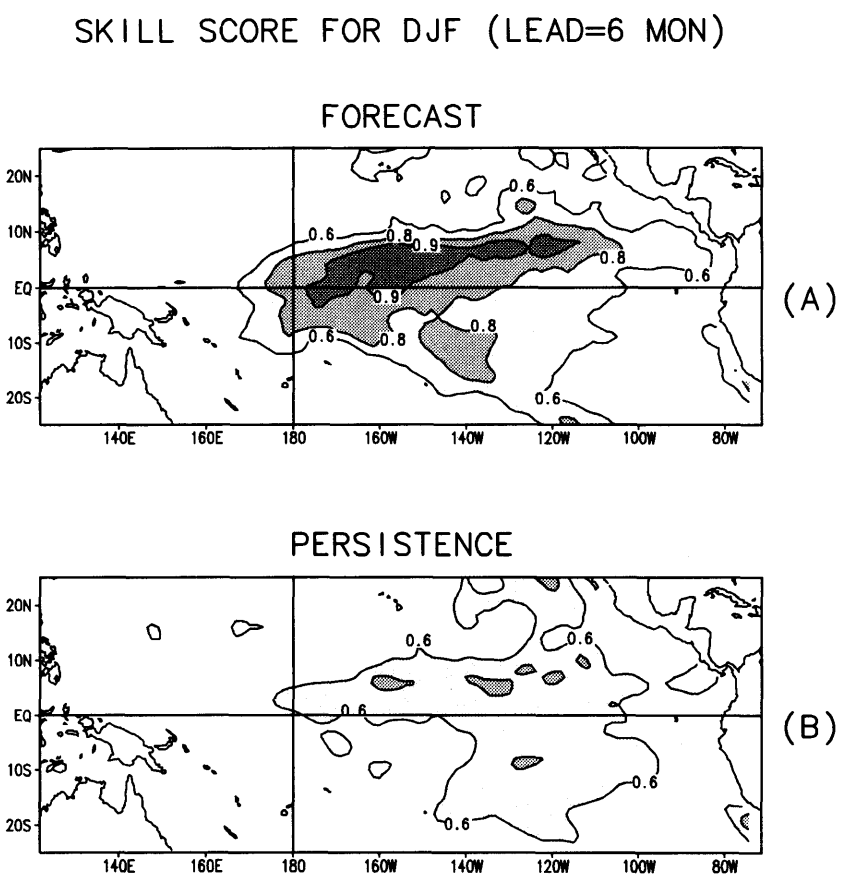

Fig. 8. The point correlation skill score for the winter season (DJF) forecasts with lead time of 6 months for the period 1984–1993 (8a). The persistence skill score which is computed by persisting the observed monthly mean SST anomaly of May, June and July through December, January and February respectively are shown in 8b. Light shading is for regions where the skill score is greater than 0.6; medium shading is for area where the skill score is greater than 0.8; and dark shading is for area where the skill score is greater than 0.9.

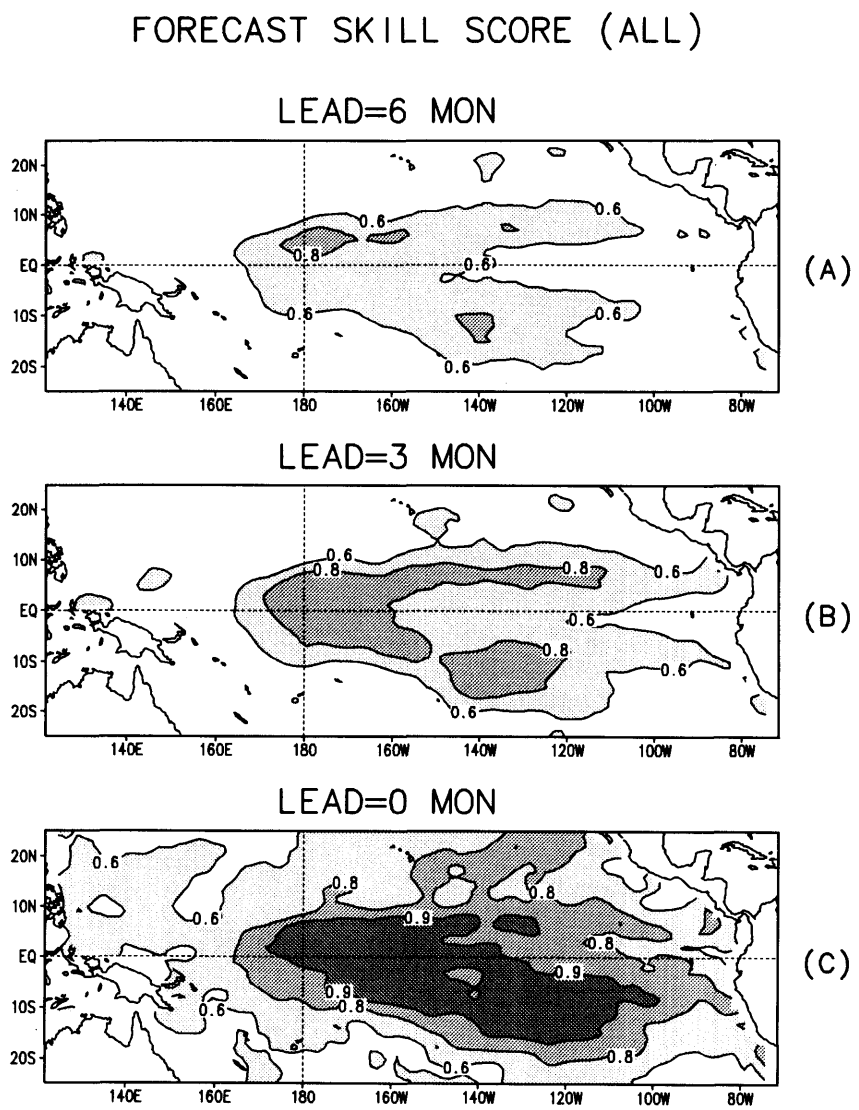

Fig. 9. The point correlation skill score for all forecasts with lead time of 6-month (a), 3-month (b) and zero month (c), regardless of starting month, for the period of October 1984 to 1993. Shadings are the same as in Fig. 8.

whereas at zero lead time, the coupled model forecast skill (9c) is comparable to the persistence skill (10c).

5. Forecast results for the Niño-3 region

Much of the previous work, which has been strongly influenced by the routine forecasts using simple coupled model by Cane and Zebiak (Cane et al., 1986; Barnett et al., 1988) for the Niño-3 area in the central/eastern Pacific. Shown in Fig. 11a are anomaly correlation coefficients (ACC) for the Niño-3 region as function of the forecast lag for all the forecasts from October 1983 to 1993. The ACCs are computed using ensemble average of forecasts starting from three consecutive months. This is to reduce the variability of

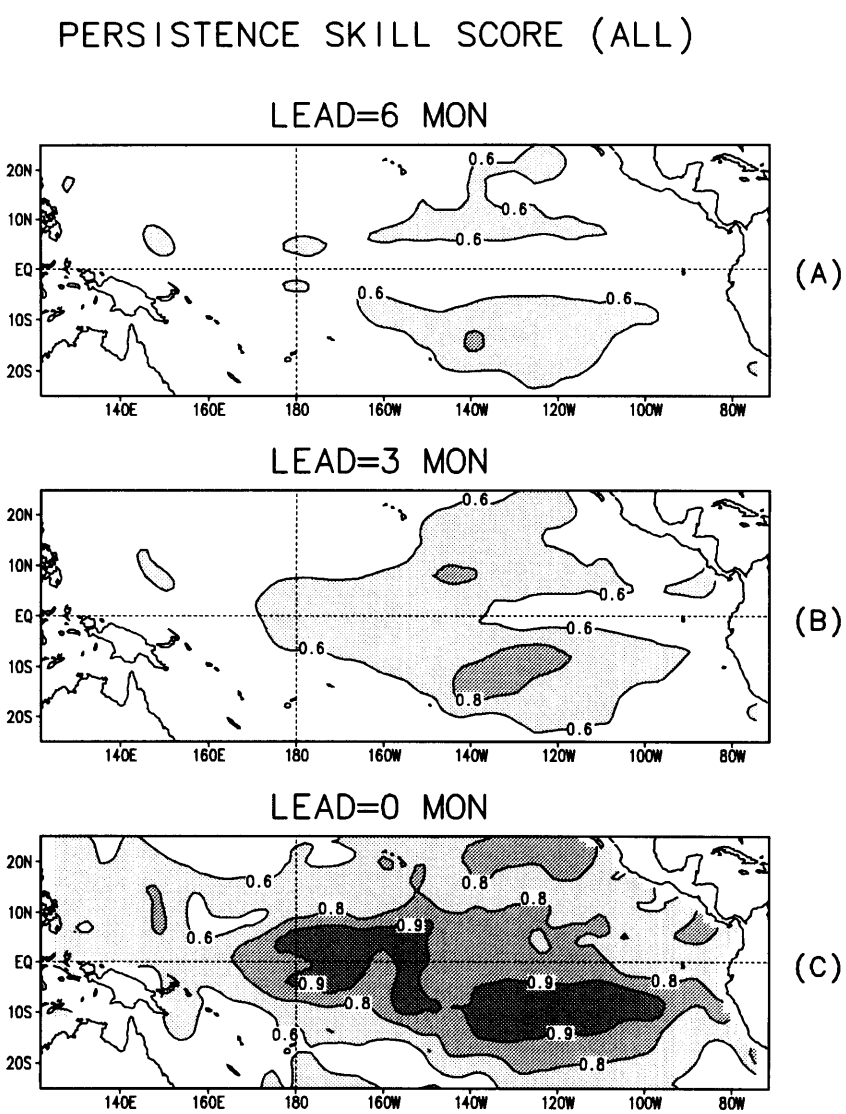

Fig. 10. Same as in Fig. 9, but for persistence forecasts. Shadings are the same as in Fig. 8.

forecasts from individual predictions. The solid curve in the figure represents ACCs computed using the coupled model forecasts, and the dotted curve in the figure represents the ACCs computed using persistence forecast which is to persist the observed SST anomaly at the initial time of a forecast and use it as forecast SST anomaly through out the forecast period. A one month lag in the figure for the coupled model represents the first month forecast; while for the persistence it represents the lag 1 auto correlation coefficient.

Fig. 11a indicates that forecasts from our coupled model consistently out performs the persistence forecasts even within the first a few month of forecasts. In contrast, coupled models that do not initialize from analyzed ocean initial conditions do not out perform the persistence forecast during early period of forecasts (Latif et al., 1993;

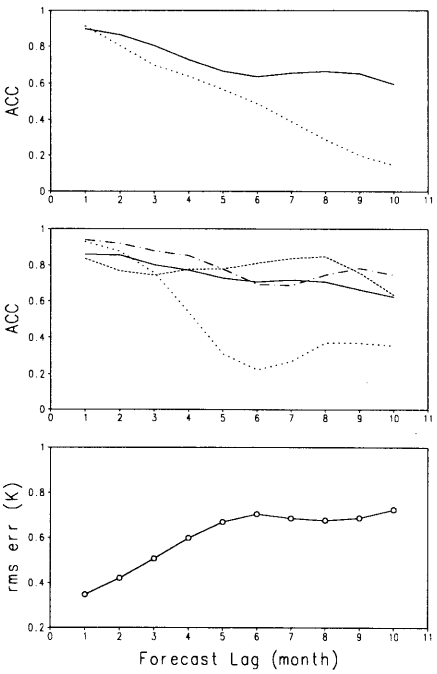

Fig. 11. Forecast skill (ACC) for the Niño-3 region SST anomalies for (a) all forecasts regardless of forecast starting month; (b) forecasts starting from different seasons. (See text). The growth of the forecast errors (r.m.s. error) for all forecasts is shown in 11c.

Neelin et al., 1994). This demonstrates the impact of the ocean data assimilation system to the forecast of climate variabilities.

Shown in Fig. 11b are the ACCs computed from forecasts starting in spring season (March to May, solid curve); summer season (June to August, dashed curve); fall season (September to November, dot-dashed curve); and winter season (December to February, dotted curve). To better represent the possible seasonality of coupled model forecasts, there is no averaging of forecasts from different starting month. The obvious feature in the figure is that skills (ACCs) for forecasts starting in winter months reduces rapidly after spring season. This rapid decrease in the ACC when forecast through northern hemisphere spring season is similar to what experienced by many other coupled models known as the "spring prediction barrier" (Latif et al., 1994). However, forecast skill may partially recover after the spring season. The exactly cause of this phenomenon has been a subject of many studies (Zebiak and Cane, 1987; Battisti, 1988; Blumentahl, 1991; Latif et al., 1994). A possible explanation of what happened in our coupled model is that during the spring season, SST is relatively warm over the central and eastern Pacific, the basin scale east–west SST gradient and the north–south SST gradient over the eastern Pacific are reduced. This could result in a much higher variability in the forcing fields (stress and heat fluxes) produced from the atmosphere model. Since the mixed layer in the eastern Pacific is shallow in general, and the upwelling is weak in the spring, a relatively small amount of heat flux error could also result in large SST errors. On the other hand, forecasts initiated from spring season for our model did not show obvious effect of the spring prediction barrier as some other coupled models did. This is probably because our forecasts are initiated from analyzed ocean initial conditions, therefore model errors are small during the first a few month of forecast despite possible large forcing errors in the spring season.

To better estimate the over all quality of the forecasts and the error growth characteristics as function of forecast length, we sort differences between the monthly forecasts and observations according to the forecast lead time regardless starting months of the forecasts. The root mean square (r.m.s.) difference for each forecast lag from 1 to 10 months are computed and depicted in Fig. 11c. This figure indicates that after an steady error growth during the 1st 5 months of integration, the forecast errors of our model for the Niño-3 region stays around 0.7°C for forecasts of up to 10 months.

Examples of our coupled model forecasts for the Niño-3 region mean SST anomalies for forecast lag of three month, six month and nine month from 1984 to 1993 are shown in Fig. 12. In each of these examples the observed SST anomaly is shown in dashed curve, the forecast SST anomaly from the coupled model is shown in solid curve. Anomaly correlation coefficients and r.m.s. difference between forecasts and observations are indicated in the figure. Forecast results for every month shown in this figure are ensemble average of forecasts starting from three consecutive months. For example, 6-month lag forecast for December 1992 is obtained by averaging forecast results for this month from forecasts starting on the first of May, June and July of 1992, respectively. By and large, the low-frequency inter-annual variations of

the SST during this period is captured well by the coupled model forecasts even at 9-month forecast lag. Noticeable SST variations during the period are: gradual warming from 1984 to 1987 and from 1988 to 1992; Major coolings in 1988 and to a less extend, in 1992; and a warming in 1993. All these features are reasonably reproduced by the coupled model. The El Niño events of 1986–87, 1991–92 and spring 1993 , and the cold event of 1988–89 are all predicted well by our coupled model at least to some extend. There are also several obvious failures of the model. The longer lag forecasts (six

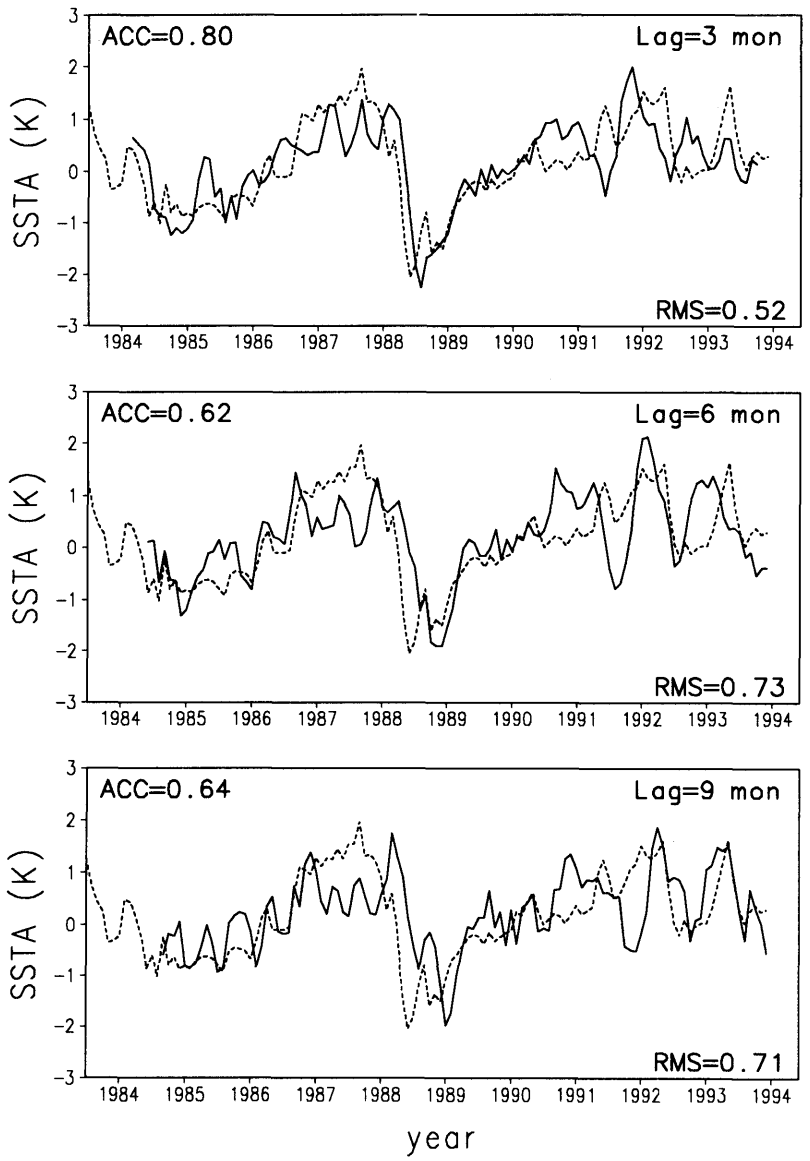

Fig. 12. Forecast and observed Niño-3 region SST anomalies for 1984–1993 for (a) 3-month lead forecasts; (b) 6-month lead forecasts; and (c) 9-month lead forecasts. Observed SST anomalies are shown in dashed curves and forecast SST anomalies are shown in solid curves. The anomaly correlation coefficients and the r.m.s. difference between the forecasts and the observations are indicated.

and nine month lag) significantly under estimated the warm SST anomaly during 1987; they also predicted a spurious cooling for fall of 1992; the 6-month lag forecast also predicted the spring 1993 warming one season too early.

6. Summary

Because of the much larger heat capacity of the ocean and because of the dominance of quasi-linear dynamics in the tropical oceans, the primary memory of the climate system on seasonal to interannual time scales lies in the ocean. Hence, knowing the ocean initial conditions is a key element of a coupled forecast system. Procedures for initializing the ocean are already well established at NMC. Routine weekly analyses based on an ocean general circulation model integrated with a four dimensional data assimilation system, which assimilates near real time surface and subsurface thermal data into the ocean, have been produced for a number of years for the Pacific and Atlantic basins for the upper ocean. Two reanalyses of the Pacific ocean for 1982 to 1992 have been completed in order to provide ocean initial conditions for coupled model hindcast experiments.

Results from the initial coupled forecast experiments, using the ocean initial conditions from the Pacific reanalyses and a T40 climate version of NMC's operational global spectral model, are presented in this paper. Results from the experimental coupled model forecasts show that the system is capable of forecasting near-equatorial SST anomalies for both the northern winter and summer seasons with lead times of 2 to 3 seasons. The r.m.s. errors in the Niño-3 index area are around 0.7°C for ensembles of 3 forecasts. For comparison, the Cane and Zebiak model shows errors in the order of 0.6–1.0°C for ensembles of 6 forecasts.

Most of the skill in the current forecast system lies in the central Pacific, to the west of the core of the Niño-3 region, between 10°N and 10°S which is similar to that found by Barnett et al. (1993). Having skill in this region is necessary in order to get the tropical convection to move to this region. This is a prerequisite in order to have a coupled system which will be able to simulate the tropical to mid-latitude teleconnections. Studies in progress and the work of others (Barnett et al., 1991) have shown that the primary mechanisms at work here to generate the anomalous temperatures are a reduction in the meridional currents and subsequently the upwelling. These result from a reduction in the easterlies. Hence at least to zero order our coupled system is simulating that part of the observed coupled interactions. The reduction of skill further to the east could have several causes. In these experiments the subsurface thermal structure did not show the amplitude of the response as is observed. Hence one can suspect that the remotely forced aspects are not as well done in this model as they need to be.

Subsequent improvements have lead to an atmospheric model which simulates the tropical to mid-latitude teleconnections associated with SST variability with significantly improved robustness. Work is currently underway to implement an end to end climate forecast system and establish its capability in forecasting tropical and mid-latitude climatic variability.

REFERENCES

Barnett, T. P., Graham, N. E., Cane, M. A., Zebiak, S. E., Dolan, S. C., O'Brien, J. J. and Legeler, P. M. 1988. On the prediction of the El Niño of 1986–87. *Science* **241**, 192–96.

Barnett, T. P., Latif, M., Krik, E. and Roecken, E. 1991. On ENSO physics. *J. Climate* **4**, 487–515.

Barnett, T. P., Latif, M., Graham, N., Flugel, M., Pazan, S. and White, W. 1993. ENSO and ENSO-related predictability: Part 1: Prediction of equatorial Pacific sea surface temperatures with a hybrid coupled ocean-atmosphere model. *J. Climate* **6**, 1545–1566.

Barnston, A. G. and Ropelewski, C. F. 1992. Prediction of ENSO episodes using canonical correlation analysis. *J. Climate* **5**, 1316–1345.

Battisti, D. S. 1988. Dynamics and thermodynamics of a warming event in a coupled tropical atmosphere-ocean model. *J. Atmos. Sci.* **45**, 2889–2919.

Blumenthal, M. B. 1991. Predictability of a coupled ocean-atmosphere model. *J. Climate* **4**, 766–784.

Boyle, J. S. 1993. Sensitivity of dynamical quantities to horizontal resolution for a climate simulation using the ECMWF (Cycle 33) model. *J. Climate* **6**, 796–815.

Bryan, K. 1969. A numerical method for the study of the world ocean. *J. Comput. Phys.* **4**, 347–376.

Cane, M. A. and Zebiak, S. E. 1985. A theory for El Niño and the Southern Oscillation. *Science* **228**, 1085–87.

Cane, M. A., Zebiak, S. E. and Dolan, S. C. 1986. Experimental forecasts of El Niño. *Nature* **321**, 827–832.

Cox, M. D. 1984. A primitive, 3-dimensional model of the ocean. *GFDL ocean group Tech. Rep. no. 1*, Geophysical Fluid Dynamics Laboratory, 143 pp.

Ebisuzaki, W. and Van den Dool, H. M. 1993a. Analysis of the variability in a GCM forced by realistically varying SST. *Proceedings of the Workshop on numerical extended range weather prediction*, 8–10 June 1993, Airlie, Virginia.

Ebisuzaki, W. and Van den Dool, H. M. 1993b. NMC Office note 402. *The atmospheric model intercomparison project at the National Meteorological Center.* Available from the National Meteorological Center, 5200 Auth Road, Camp Springs, Md. 20746 USA.

Hartmann, D. L., Hendon, H. H. and Houze, R. A. Jr. 1984. Some implications of the mesoscale circulations in the tropical cloud clusters for large-scale dynamics and climate. *J. Atmos. Science* **41**, 113–121.

Harrison, D. E. 1989. On climatological mean wind stress and wind stress curl fields over the world ocean. *J. Climate* **2**, 57–70.

Hellerman, S. and Rosenstein, M. 1983. Normal monthly wind stress over the world ocean with error estimates. *J. Phys. Oceanogr.* **13**, 1093–1104.

Holtslag, A. A. M. and Moeng, C.-H. 1991. Eddy diffusivity and countergradient transport in the convective atmospheric boundary layer. *J. Atmos. Sci.* **48**, 1690–1698.

Ji, M., Kumar, A. and Leetmaa, A. 1994a. A multi-season climate forecast system at the National Meteorological Center. *Bull. of Amer. Meteor. Soc.*, in press.

Ji, M., Leetmaa, A. and Derber, J. 1994b. An ocean analysis system for climate studies. *Mon. Wea. Rev.*, in press.

Kanamitsu, M. 1989. Description of the NMC global data assimilating and forecast system. *Weather and Forecasting* **4**, 335–442.

Kanamitsu, M., Mo, K. C. and Kalnay, E. 1990. Annual cycle integration of the NMC medium range forecasting (MRF) model. *Mon. Wea. Rev.* **118**, 2543–2567.

Kanamitsu, M., Mo, K. C., Kalnay, E., Alpert, J. C., Campana, K. A., Caplan, P. M., Deaven, D. G., Iredell, M., Katz, B., Pan, H. L., Sella, J. and White, G. H. 1991. Recent changes implemented into the global forecast system at NMC. *Weather and Forecasting* **6**, 425–435.

Kim, J. and Mahrt, L. 1992. Simple formulation of turbulent mixing in stable free atmosphere and nocturnal boundary layer. *Tellus* **44A**, 381–394.

Kloesel, K. A. and Albrecht, B. A. 1989. Low-level inversions over the tropical Pacific: Thermodynamic structure of the boundary layer and the above-inversion moisture structure. *Mon. Wea. Rev.* **117**, 87–101.

Latif, M., Sterl, A., Maier-Reimer, E. and Junge, M. M. 1993. Structure and predictability of the El Niño/Southern Oscillation phenomenon in a coupled ocean-atmosphere general circulation model. *J. Climate* **6**, 700–708.

Latif, M., Barnett, T. P., Cane, M. A., Flugel, M. and Graham, N. E. 1994. A review on ENSO prediction studies. *Climate Dyn.* **9**, 167–179.

Lau, K.-M. and Peng, L. 1987. Origin of the low-frequency (intra-seasonal) oscillations in the tropical atmosphere: Part 1: Basic theory. *J. Atmos. Science* **44**, 950–972.

Leetmaa, A. and Ji, M. 1989. Operational hindcasting of the tropical Pacific. *Dyn. Atmos. Oceans* **13**, 465–490.

Lindzen, R. S. and Nigam, S. 1987. On the role of sea surface temperature gradients in forcing low level winds and convergence in the tropics. *J. Atmos. Science* **44**, 2418–2436.

McCreary, J. P. and Anderson, D. L. T. 1984. A simple model of El Niño and the Southern Oscillation. *Mon. Wea. Rev.* **112**, 934–46.

Meehl, G. A. and Albrecht, B. A. 1991. Response of a GCM with a hybrid convection scheme to a tropical Pacific sea surface temperature anomaly. *J. Climate* **4**, 672–688.

Neelin, J. D. 1988. A simple model for surface stress and low-level flow in the tropical atmosphere driven by prescribed heating. *Quat. J. Roy. Meteo. Soc.* **114**, 747–770.

Neelin, J. D. and Held, I. M. 1987. Modeling tropical convergence based on the moist static energy budget. *Mon. Wea. Rev.* **115**, 3–12.

Neelin, J. D., Latif, M. and Jin, F.-F. 1994. Dynamics of coupled ocean-atmosphere models: The tropical problem. *Annu. Rev. Fluid Mech.* **26**, 617–659.

NMC Staff, 1988. Documentation of the research version of NMC medium range forecasting model. [Available from NOAA/NMC, Development Division, Washington, DC 20233]

Pacanowski, R. and Philander, S. G. H. 1981. Parameterization of vertical mixing in numerical models of tropical oceans. *J. Phys. Oceanogr.* **11**, 1443–1451.

Philander, S. G. H., Hurlin, W. J. and Seigel, A. D. 1987. A model of the seasonal cycle in the tropical Pacific ocean. *J. Phys. Oceanogr.* **17**, 1986–2002.

Philander, S. G. H., Lau, N. C., Pacanowski, R. C. and Nath, M. J. 1989. Two different simulations of Southern Oscillation and El Niño with coupled ocean-atmosphere general circulation models. *Phil. Trans. Roy. Soc. Lond.* **A329**, 167–78.

Reed, R. K. 1977. On Estimating insolation over the ocean. *J. Phys. Oceanogr.* **6**, 781–800.

Reynolds, R. W. 1988. A real-time global sea surface temperature analysis. *J. Climate* **1**, 75–86.

Reynolds, R. W. and Marsico, D. C. 1993. An improved real-time global sea surface temperature analysis. *J. Climate* **6**, 114–119.

Reynolds, R. W., Arpe, K., Gordon, C., Hayes, S. P., Leetmaa, A. and McPhaden, M. J. 1989. A comparison of tropical pacific surface wind analyses. *J. Climate* **2**, 105–111.

Schopf, P. S. and Suarez, M. J. 1988. Vacillations in a coupled ocean-atmosphere model. *J. Atmos. Science* **45**, 549–566.

Slingo, A. and Slingo, J. M. 1991. Response of the National Center for Atmospheric Research community climate model to improvements in the representation of clouds. *J. Geophys. Res.* **96**, 15341–15357.

Sud, Y. C., Chao, W. C. and Walker, G. K. 1991. Contributions to the implementation of the Arakawa-Schubert cumulus parameterization in the GLA GCM. *J. Atmos. Sci.* **48**, 1573–1586.

Tibaldi, S., Palmer, T. N., Brankovic, C. and Cubasch, U. 1990. Extended-range prediction with ECMWF models: Influence of horizontal resolution on systematic error and forecast skill. *Quat. J. Roy. Meteo. Soc.* **116**, 835–866.

Troen, I. and Mahrt, L. 1986. A simple model of the atmospheric boundary layer: Sensitivity to the surface evaporation. *Bound. Layer Meteo.* **37**, 129–148.

Van den Dool, H. M. and Saha, S. 1993. On the seasonal redistribution of mass in a 10-year GCM run. *J. Climate* **6**, 22–30.

Wyrtki, K. 1975. El Niño: The dynamical response of the equatorial Pacific to atmospheric forcing. *J. Phys. Ocean.* **5**, 572–584.

Wyrtki, K. 1985. Water displacements in the Pacific and the genesis of El Niño cycles. *J. Geophy. Res.* **90**, C4, 7129–32.

Zebiak, S. E. and Cane, M. A. 1987. A model El Niño-Southern Oscillation. *Mon. Weather Rev.* **115**, 2262–2278.